Condition Monitoring of Wound Field Synchronous Generator under Inter-turn Short Circuit Fault utilizing Vibration Signal

Hossein Ehya*, Gaute Lyng Rødal*, Arne Nysveen*, and Robert Nilssen*
* Department of Electrical Power Engineering, Norwegian University of Science and Technology, 7030 Trondheim, Norway

***Abstract*—In this paper, a novel frequency index for Inter Turn Short Circuit (ITSC) fault diagnosis of the Wound Field Synchronous Generator (WFSG) is presented by utilizing the air gap flux density and the total force density. The analytical expression of the force density is derived to detect the sideband harmonics of the vibration in the faulty WFSG by considering the impacts of rotor saliency, saturation, stator slots, and ITSC fault. The 2-D finite element method is employed to extract the characteristics of the faulty machine. The harmonic force response of the healthy and faulty WFSG acquired from the magnetic analysis is used as an input to the mechanical analysis to get the deformation, modal analysis of faulty WFSG.**

***Index Terms*— Condition monitoring, Inter-turn short circuit fault, vibration, wound field synchronous generator.**

NOMENCLATURE

b	magnetic flux density
C_c	Carter's coefficient
f_s	synchronous electrical frequency
f_r	force density in a radial direction
f_t	force density in a tangential direction
f_{rr}	radial force density
F	magnetomotive force (MMF)
g	air-gap function
g_0	nominal air-gap length
J	current density
k	order of time-harmonic
k_{sat}	saturation factor
L_s	stator stack length
m	mode number
p	number of pole pairs
Q_s	number of slots
α_1, α_2	geometry coefficient of salient poles
θ_r	angular mechanical position of the rotor
Λ	air gap permeance
μ_0	permeability of free space
ϕ	angle along an inner surface of the stator
ϕ_r	angle in the rotor reference plane
ω_s	angular electrical synchronous frequency
ω_r	angular velocity of rotor
v_i	integer number
F_{tooth}	force acting on stator tooth

This work was supported by Norwegian Hydropower Centre (NVKS) and Norwegian Research Centre for Hydropower Technology.

I. INTRODUCTION

A short circuit caused by insulation defect is one of the most common faults in synchronous generators, accounting for more than 40% of all faults [1-2]. The winding insulation deteriorates over time due to thermal, electrical, and mechanical stresses, as well as aging and contamination, which normally results in insulation breakdown. This process can be accelerated by sub-optimal operating conditions such as thermal cycling caused by frequent load variations, excessive vibration, or overheating due to overloading or insufficient cooling. Additionally, other generator faults such as broken damper bars and eccentricity can lead to local temperature rise in the rotor core and increased thermal stress on the field winding insulation. Short circuits in the field winding can happen between a turn and a grounded point, called a ground fault, or between turns, called an inter-turn fault.

As the insulation between turns usually degrades before the insulation between conductors and ground, inter-turn faults are more common than ground faults. A single ITSC may not be critical for the machine and may be present without affecting the generator performance to a noticeable degree. When an ITSC occurs, the number of ampere-turns in the affected pole is decreased, which weakens the MMF and magnetic field produced by that pole. Thus, the effect of one short circuit will depend on the total number of ampere-turns per pole. The generators with few rotor turns will suffer relatively larger consequences than generators with more turns.

The weakened magnetic field produced by a pole with an ITSC causes an asymmetrical air-gap field resulting in distorted force distribution and possibly increased vibration. The airgap forces in a generator are attracting the stator towards the rotor. The modified force distribution caused by an ITSC leads to an unbalanced magnetic pull (UMP). UMP may increase the vibration level of the generator intensifying the mechanical stress on the winding insulation. Additionally, uneven distribution of losses in the coil due to a short circuit changes the rotor heating pattern, leading to increased thermal stress. Non-uniform rotor temperature may also develop shaft bowing and further increased UMP. These consequences can aggravate the fault by short-circuiting

several turns, which will further amplify the UMP. Hence, even a single ITSC with a minor impact on the generator's operation may develop into a highly destructive fault.

Electrical or mechanical faults in synchronous generators affect the air-gap magnetic field, leading to distorted air-gap forces and change of vibration behavior. Thus, measuring vibration is an effective monitoring method that provides detailed information about the condition of the generator. With almost one hundred years of accumulated research, it is a well-established technique with standards covering a wide range of electrical machines [3].

The vast development of hardware and software during the last decades has enabled the usage of advanced measurement equipment, signal processing tools, and artificial intelligence, which have been utilized in the detection of winding faults in stator and rotor electric machines [4-7]. However, electric signals like current, voltage, or air gap magnetic field are widely utilized for detection purposes. However, an extensive literature review revealed that most of the research on vibration in rotating electrical machines concerns asynchronous machines, and salient-pole synchronous generators have not been explored to a sufficient extent [8-17]. Further research to establish reliable methods for the detection and classification of faults in WFSG is therefore needed.

This paper presents a comprehensive study of ITSC faults and its consequences on the magnetic field and vibration of WFSG. An analytical approach for pattern recognition of the WFSG under ITSC faults is proposed. Two unique features are extracted from the analytical approach to discriminate the air gap magnetic field and the vibration frequency component. The finite element approach is used to calculate the force distribution in the healthy and faulty machine. A detailed mechanical analysis including vibration analysis and deformation are obtained based on the magnetic field distribution of a healthy, and a faulty WFSG.

II. VIBRATION IN WFSG

Vibration in rotating electrical machines is mainly caused by radial forces acting on the stator through the air gap [18]. The forces in the air gap can be decomposed into radial and tangential components, whereas the tangential component creates useful electromagnetic torque and forms the basis for power generation, the radial component is the reason for vibration. They can be expressed as force per square meter, thereafter termed force density and calculated using the Maxwell stress tensor according to Eq. 1 in the tangential direction and Eq. 2 in the radial direction as below:

$$f_t = \frac{1}{\mu_0}(b_r b_t) \tag{1}$$

$$f_r = \frac{1}{2\mu_0}(b_r^2 - b_t^2) \tag{2}$$

where b_r and b_t represent the radial and tangential component of the air-gap magnetic flux density, respectively. Due to the small air-gap length in rotating electrical machines, and the fact that the magnetic permeability of the rotor and stator iron is much higher than in air, the air-gap flux density is dominated by the radial component. Consequently, b_t has traditionally been neglected in analytical calculations of the radial air-gap forces [18]. More recent studies have shown that the tangential component can cause a noteworthy impact on radial force calculation in large round-rotor permanent-magnet machines with open slots [19].

In general, the radial force density can be expressed as equation Eq. 3, where f_r is a radial force density wave that causes attraction between the rotor and the stator, and it rotates in the air gap with an angular speed of $k\omega_r/m$, either in the same or opposite direction of the rotor [18]. It acts on the stator teeth surface that faces the air gap and a total tooth force propagates into the stator yoke where it can cause significant deformations. The total force acting on a tooth can be calculated by integrating the force density over the tooth line, L_t, and multiplying with the stator stack length, L_s, as shown in Eq. 4.

$$f_r(\phi, t) = F\ cos(k\omega_r t - m\phi) \tag{3}$$

$$F_{tooth} = L_s \int_{L_t} f_r\, dl \tag{4}$$

The forces of low spatial harmonic orders normally cause the worst vibration due to their impact on the mechanical deformation in the stator. The number of identical magnetic parts of the generator is crucial for the lowest spatial periodicity of the forces and, consequently, the lowest harmonic order. This number can be determined based on the generator's number of stator slots and rotor poles [20]. Specifically, the lowest non-zero order that occurs naturally in a generator in no-load operation is equal to the greatest common divisor (GCD) between the number of slots and the number of poles. Thus, some generators can have a spatial harmonic of low order due to their topology and potentially a high vibration level even during healthy operation. This coherence may be different during loaded operation for some generators.

III. ANALYTICAL MODELING

Using processing tools to extract the frequency content of an acquired vibration signal is an important part of condition monitoring and knowing which frequency components must present in the spectrum of a signal is essential. Such knowledge can be obtained by developing analytical models that describe the vibration-producing forces mathematically. In this section, the forces in a WFSG under an ITSC fault has been analytically modeled by using a permeance-wave method. The permeance-wave method treats the airgap permeance, MMF, and flux density as circumferential distributed along the air gap such that they can be modeled and

expressed as waves. Thereafter, the Maxwell stress tensor and the tooth line integration can be utilized to calculate the radial force density and the total force. The saliency of the rotor poles, the geometry of the stator slots, the effects of iron saturation, and the impact of ITSC in the field winding are considered in the extracted analytical method. The section is divided into several subsections for the stepwise formulation of the air gap magnetic density and total force, to determine orders of the time and spatial harmonics that influence the vibration in a generator stator. These calculations are one-dimensional and only the radial direction has been analyzed since the tangential component of the flux density is assumed to be relatively negligible.

A. Air gap Function

For round rotors, the air-gap length, g_0, is a constant in healthy condition, while air gap function in salient-pole machines varies due to the rotor saliency which is described as below [21, 22]:

$$g_0(\phi,t)=\frac{1}{\alpha_1+\alpha_2 cos(2p(\theta_r-\phi))} \tag{5}$$

The slotted stator causes uneven reluctance in the air gap. The increased reluctance and air gap length caused by the slot openings have been incorporated into the air gap function by the Carter coefficient [18]. The air gap function by considering the slotting effects is as below:

$$g_{ss}(\phi,t)=\frac{\tau}{\tau-\frac{W_{ss}^2/g_0}{5W_{ss}+W_{ss}^2/g_0}}\cdot g_0. \tag{6}$$

The flux passes through the stator teeth may cause magnetic saturation. Saturation decreases the relative permeability of iron and increases its reluctance, which has been considered the air-gap function. As the air gap has a constant relative permeability of μ_0, the gap length has been modified to accommodate the reluctance variation due to saturation, which is commonly done by modulation of the air-gap function with twice the number of poles and twice the frequency of the fundamental flux density wave [18]. Hence, the air-gap function considering the saturation effect of the teeth becomes:

$$g_{sat}(\phi,t)=g_{ss}\left(k_m-k_e cos(2\omega_s t-2p\phi)\right) \tag{7}$$

where the coefficients k_m and k_e are as below:

$$k_m=\frac{3k_{sat}}{k_{sat}+2},\ k_e=\frac{2k_{sat}-2}{3k_{sat}} \tag{8}$$

where saturation factor, k_{sat}, is the ratio of the fundamental component of no-load to full-load line voltage [21]. The air-gap function of a WFSG considering rotor saliency, stator slotting effect and the saturation effects is written as below:

$$g(\phi,t)=g_{sat}(\phi,t)=\frac{C_c(k_m-k_e cos(2\omega_s-2p\phi))}{\alpha_1+\alpha_2 cos(2p(\frac{\omega_s t}{p}-\phi))} \tag{9}$$

B. Air gap Permeance

The airgap permeance considering saliency of the rotor pole, slotting and saturation effect is:

$$\Lambda=\frac{\mu_0}{g_{sc}}=\frac{\mu_0(\alpha_1+\alpha_2 cos(2\omega_s t-2p\phi))}{C_c(k_m-k_e cos(2\omega_s t-2p\phi))} \tag{10}$$

Taylor series expansion of Eq. 10 has been simplified as below:

$$\Lambda=\sum_{\upsilon_1,\upsilon_2}\Lambda cos((2\upsilon_1+2)\omega_s t-2p(\upsilon_2\pm1)\phi). \tag{11}$$

C. MMF

The stator MMF by considering the sinusoidal current density feed into winding is as below:

$$F_{sc}^s(\phi,t)=\oint J^s sin(\omega_s t-p\phi)d\phi=\frac{J^s}{p}cos(\omega_s t-p\phi). \tag{12}$$

However, when there is an ITSC in the rotor winding, the MMF produced by the pole with faulty winding is reduced. The resulting rotor MMF has been formulated by superimposing the original MMF field, F_h, and a demagnetizing component caused by the short circuit, F_f.

$$\begin{aligned}F_{sc}^r(\phi,t)&=F_h(\phi,t)+F_f(\phi,t)\\&=\frac{J^r}{p}cos(\omega_s t-p\phi)+\sum_{n=1}^{\infty}F_{f,n}cos\left(\frac{n}{p}\omega_s t-n\phi\right)\end{aligned} \tag{13}$$

D. Magnetic Flux Density

The air-gap magnetic flux density was obtained by multiplication of the air gap permeance and MMF. The flux density produced by the armature during operation with a short circuit in the rotor is the same as for healthy operation and has been calculated in the following way:

$$\begin{aligned}b_{sc}^s(\phi,t)&=\Lambda_{sc}(\phi,t)\cdot F_{sc}^s(\phi,t)\\&=\sum_{\upsilon_1,\upsilon_2}B_{sc}^s cos((2\upsilon_1+1)\omega_s t-((2\upsilon_2+1)p\pm2p)\phi).\end{aligned} \tag{14}$$

For the rotor, the modified MMF field due to the short circuit fault has been considered which resulted in:

$$\begin{aligned}b_{sc}^r(\phi,t)&=\Lambda_{sc}(\phi,t)\cdot F_{sc}^r(\phi,t)=\\&=\sum_{\upsilon_1,\ldots,\upsilon_4}^{\infty}B_{sc}^r cos\left(\left(2\upsilon_1\pm\frac{\upsilon_2}{p}\right)\omega_s t-(2p\upsilon_3\pm\upsilon_4)\phi\right)\end{aligned} \tag{15}$$

The combination of Eq. 14, and Eq. 15 forms the resultant flux density under rotor ITSC as follows:

$$\begin{aligned}b_{sc}(\phi,t)&=b_{sc}^s(\phi,t)+b_{sc}^r(\phi,t)\\&=\sum_{\upsilon_1,\ldots,\upsilon_4}B_{sc}cos\left(\left(2\upsilon_1\pm\frac{\upsilon_2}{p}\right)\omega_s t-(2p\upsilon_3\pm\upsilon_4)\phi\right)\end{aligned} \tag{16}$$

The following frequency pattern in a case of ITSC fault can be extracted from the air gap magnetic field as below:

$$F_{fault}=\left(2\upsilon_1\pm\frac{\upsilon_2}{p}\right)f_s \tag{17}$$

TABLE I
DETAILED SPECIFICATION OF 100 KVA, 400 V, WFSG

Nominal current	144.3 A	Number of slots	114
Nominal speed	428.6 RPM	Damper bars per pole	7
Nominal frequency	50 Hz	Outer rotor diameter	646.5
Nominal Power factor	0.9	Air-gap length	1.75
No-load exc. current	53.2 A	Outer stator diameter	780
Nominal exc. current	103 A	Number of poles	14
Winding connection	star	GCD	2

E. Total Force Density

The radial force acting on the machine is derived based on the radial magnetic field as below:

$$f_{sc}(\phi,t)=\frac{b_{sc}^2(\phi,t)}{\mu_0} = \sum_{\upsilon_1,\ldots,\upsilon_4} F_{sc}\cos\left(\left(\frac{2\upsilon_1 p\pm\upsilon_1}{p}\pm 2\upsilon_2\right)\omega_s t-(p\upsilon_3\pm\upsilon_4)\phi\right) \quad (18)$$

The radial force density is the force per square meter that acts on the stator teeth. In order to calculate the total force that acts on one tooth or entire teeth, the radial force density must be multiplied with the stack length and integrated over the tooth line. The total force under ITSC fault is as below:

$$F_{sc}(\phi,t)=L_s\int f_{sc}(\phi,t)\cdot\cos(\phi)d\phi = \sum_{\upsilon_1,\ldots,\upsilon_4} F_{sc}\sin\left(\frac{2\upsilon_1 p\pm\upsilon_1}{p}\pm 2\upsilon_2\right)\omega_s t-(p\upsilon_3\pm\upsilon_4)\phi \quad (19)$$

The following frequency patterns can be used based on the total force acting on a machine for ITSC fault detection:

$$F_{fault}=\left(\frac{2\upsilon_1 p\pm\upsilon_1}{p}\pm 2\upsilon_2\right)f_s \quad (20)$$

IV. FINITE ELEMENT ANALYSIS

The accuracy of the fault detection depends on the precise modeling of the machine in the finite element (FE) environment. The detailed geometrical characteristics of the machine including, stator, and rotor slots, the spatial distribution of the winding, the saliency of the rotor pole, non-linearity of material are considered. Time-stepping FE has been performed in two software ANSYS Maxwell and Mechanical [23, 24]. Maxwell has been utilized to compute the magnetic flux density, force density, and total force in the air gap of the WFSG. The total force was later transferred to Mechanical to calculate the vibration and modal analysis. Table. I present the detailed specification of the 100 *kVA* WFSG.

A. Magnetic Field Analysis

The time-domain distribution of the radial flux density in the air gap in healthy and under ITSC fault is depicted in Fig. 1(a). Seven deep dips in each amplitude are caused by the slots where the seven damper bars of the rotor are located. These slots cause a non-uniform permeability path for the flux passing the poles which lead to decreased air-gap flux density.

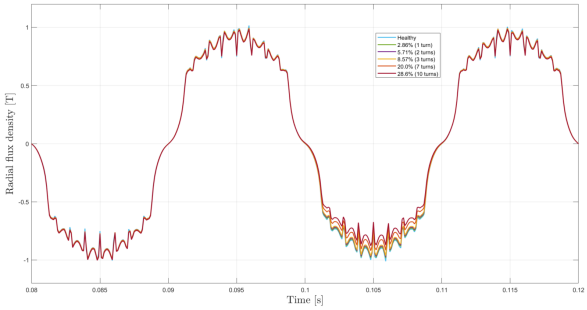

(a)

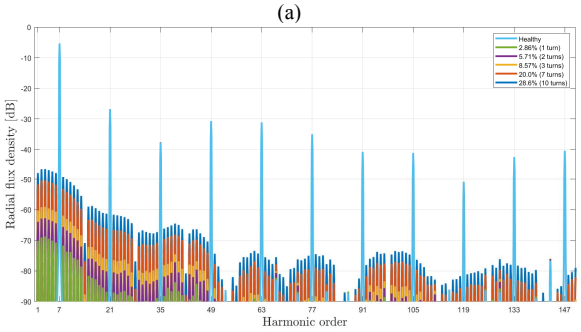

(b)

Fig. 1. The radial flux density of WFSG in healthy and under ITSC fault (a), fast Fourier transform of radial flux density (b).

The simulated fault degree varies from 1 turn up to 10 turns which are 2.86% to 28.6% of one rotor pole winding. The reduced magnetic field at the faulty pole is due to a result of the reduced ampere-turns in the faulty winding. Fig. 1(b). shows the FFT of the radial flux density in the air gap in healthy operation and for the various degrees of ITSC as extracted by Eq. 17. As seen in Fig. 1(b). ITSCs have a substantial impact on inter harmonics. The distorted periodicity of the time distribution causes induced side-band components at each natural component. The sidebands of the fundamental and all subharmonics are the most affected and amplified already after one shorted turn. Their magnitudes may indicate that their influence on the generator is not critical during low fault severities, while as the fault degree raises, they become significant compared to healthy operation. The lowest difference between the harmonic orders is one and interactions between them will excite the first-order force density harmonics, which can be critical for the vibration of the generator.

B. Magnetic Force Analysis

The radial air-gap force density is depicted in Fig. 2 (a). Maxwell stress tensor squaring the flux density, according to Eq. 2, that changes the negative flux density amplitudes to positive force density amplitudes. The squaring also makes the impact of the damper bars even more notable. The lowest value of the wave is at -32 N/m^2 which indicates that the tangential flux density component, which imposes a negative term in the Maxwell stress tensor, is insignificant. The force produced by the faulty pole is reduced as a symptom of the weakened flux field. The force wave with reduced amplitude rotates in the air gap and imposes a dynamic UMP which is significant as the fault degree raises.

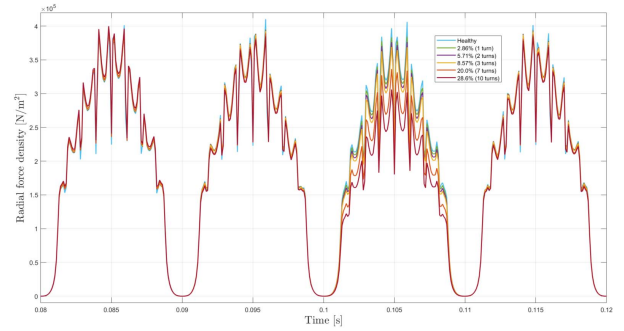

(a)

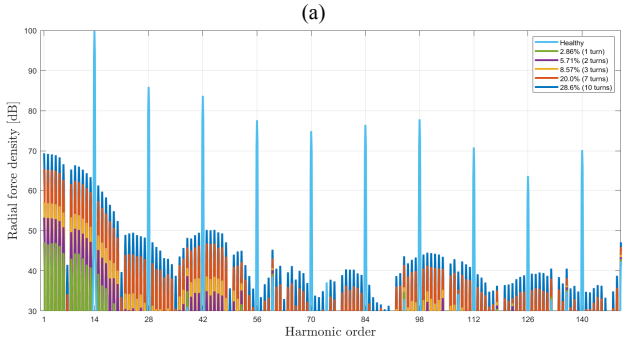

(b)

Fig. 2. Radial force density of WFSG in healthy and under ITSC fault (a), fast Fourier transform of radial force density (b).

In the frequency spectrum presented in Fig. 2 (b), the 14th harmonic is the main component. It corresponds to 100 *Hz* and twice the frequency of the fundamental flux harmonic. Natural harmonics are presented at every multiple of 100 *Hz*, caused by the interaction between natural flux density harmonics. The harmonics in the radial force density are highly affected by the ITSC fault and their frequencies are detectable by Eq. 20. The low-order force density subharmonics are results of the interaction between adjacent flux density harmonics. With a 10 ITSC, the first spatial harmonic reaches 71.7 *dB*, which corresponds to 3.8 kN/m^2. This is 4.7\% of the main component and in the same order of magnitude as the high-order natural harmonics. The resulting vibration can cause severe damage to the machine if the relatively high amplitudes of the low-order harmonics are combined with low-order spatial harmonics.

C. Mechanical Analysis

Fig. 4. shows the simulated deformation of the stator yoke during healthy and ITSC fault condition in no load. As expected, vibration at 100 *Hz* is dominating the spectrum caused by the main frequency component of the air-gap forces. The deformation at 100 *Hz* is in terms of tens of nanometers, which is negligible. However, the 100 kVA WFSG is small compared to a real hydropower generator and the magnitude of vibration may be higher for larger generators. Fig. 4 depicts a dramatic augmentation of vibration at 7.14 *Hz* during a fault. The rotor frequency vibration by having one ITSC increased approximately 6500 times from healthy conditions and the most severe fault degree produces around 80000 times higher vibration than a healthy generator at mentioned frequency.

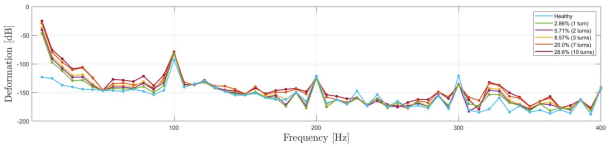

Fig. 4. The frequency spectrum of stator yoke deformation during no-load operation and under ITSC fault in the rotor winding.

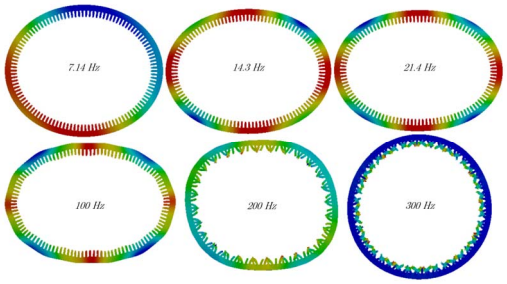

(a)

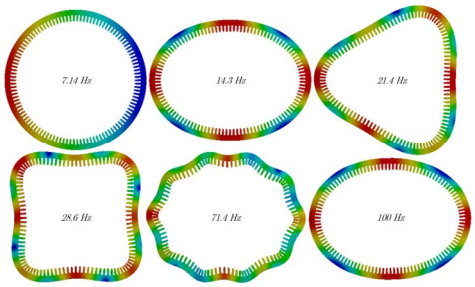

(b)

Fig. 5. Deformation profiles of the stator at healthy (a) and various frequencies during ITSC fault in the rotor winding (b).

Fig. 5 (a). shows how the stator is deformed at six different frequencies during healthy operation. All shapes were found to be equal for both no-load and full load operation. The deformation at 100 *Hz* is dominated by the second mode as the stator has two clear attraction points at the top and bottom center. The shape is not completely circularly smooth but has 14 minor indents due to the 14th spatial harmonic. This means that the air gap consists of several 100 *Hz* force density waves with different spatial harmonic orders. Although not as significant as at 100 *Hz*, the second mode is also the most prominent at 200 *Hz*. On the other hand, the second vibration mode is absent at 300 *Hz* and the twisted stator teeth may indicate that modes with more complex deformation profiles are involved. Hence, the small increase in 300 *Hz* vibration can be explained by the time domain force density harmonic at 300 *Hz*. It can be concluded that the second deformation mode is the most momentous in healthy operation.

Fig. 5(b) illustrates how the stator is deformed at six different frequencies due to ITSC fault. It shows how the time-harmonic number, k, and the spatial harmonic number, m, follow each other at low frequencies. That is, the stators at the four lowest frequencies, which correspond to k = 1, 2, 3, and 4, are solely deformed by the first, second, third, and fourth mode, respectively. Hence, the 7.14 Hz force density waves in the air gap have m=1 which explains why deformation at 7.14 Hz is

most severe even though the amplitudes of the exciting forces are more or less the same. The deformation is heavily elevated also at 14.3 Hz, 21.4 Hz, and 35.7 Hz, and in general, increased at every subharmonic frequency expect for 50 Hz. Vibration at 100 Hz is also affected by the fault.

V. Conclusions

Through analytical and FE modeling of air gap forces, this paper has investigated how vibration signals can be used for fault detection in WFSG under ITSC fault. The novel analytical model formulates unnatural time harmonics and spatial harmonics to appear at every order as a result of ITSC fault in the air gap magnetic field and force density. FE modeling of the air gap flux density and radial force density revealed that ITSC in the rotor winding excites unnatural harmonics in the time domain and the spatial domain which causes a dramatic elevation in low-frequency vibration compared to a healthy condition, specifically by over 80000 times at rotor frequency during 28.6\% ITSC fault in one rotor pole. The first order spatial harmonic cause vibration under faulty situation while it is second order in a healthy condition.

References

[1] I. Sadeghi, H. Ehya, J. Faiz, and A. A. S. Akmal, "Online condition monitoring of large synchronous generator under short circuit fault — A review," 2018 IEEE International Conference on Industrial Technology (ICIT), Lyon, 2018, pp. 1843-1848.

[2] I. Sadeghi, H. Ehya, J. Faiz and H. Ostovar, "Online fault diagnosis of large electrical machines using vibration signal-a review," 2017 International Conference on Optimization of Electrical and Electronic Equipment (OPTIM) & 2017 Intl Aegean Conference on Electrical Machines and Power Electronics (ACEMP), Brasov, 2017.

[3] Tavner, Peter, et al. 'Condition monitoring of rotating electrical machines.' Vol. 56. IET, 2008.

[4] M. Cuevas, R. Romary, J. Lecointe, and T. Jacq, "Non-Invasive Detection of Rotor Short-Circuit Fault in Synchronous Machines by Analysis of Stray Magnetic Field and Frame Vibrations," in IEEE Transactions on Magnetics, vol. 52, no. 7, pp. 1-4, July 2016.

[5] S. Nadarajan, R. Wang, A. Kumar Gupta, and S. Kumar Panda, "Vibration signature analysis of stator winding fault diagnosis in brushless synchronous generators," 2015 IEEE International Transportation Electrification Conference (ITEC), Chennai, 2015, pp. 1-6.

[6] S. Djurović, D. S. Vilchis-Rodriguez, and A. C. Smith, "Investigation of wound rotor induction machine vibration signal under stator electrical fault conditions," in The Journal of Engineering, vol. 2014, no. 5, pp. 248-258, 5 2014.

[7] J. R. Cameron, W. T. Thomson, and A. B. Dow, "Vibration and current monitoring for detecting airgap eccentricity in large induction motors," in IEE Proceedings B - Electric Power Applications, vol. 133, no. 3, pp. 155-163, May 1986.

[8] D. G. Dorrell, W. T. Thomson, and S. Roach, "Analysis of airgap flux, current, and vibration signals as a function of the combination of static and dynamic airgap eccentricity in 3-phase induction motors," in IEEE Transactions on Industry Applications, vol. 33, no. 1, pp. 24-34, Jan.-Feb. 1997.

[9] G. Rødal, 'Online condition monitoring of synchronous generators using vibration signal', Master thesis, Dept. of Electric Power Engineering, NTNU, Trondheim, 2020.

[10] M. Cuevas, R. Romary, J. Lecointe, and T. Jacq, "Non-Invasive Detection of Rotor Short-Circuit Fault in Synchronous Machines by Analysis of Stray Magnetic Field and Frame Vibrations," in IEEE Transactions on Magnetics, vol. 52, no. 7, pp. 1-4, July 2016.

[11] M. Cuevas, R. Romary, J. Lecointe, F. Morganti, and T. Jacq, "Noninvasive Detection of Winding Short-Circuit Faults in Salient Pole Synchronous Machine With Squirrel-Cage Damper," in IEEE Transactions on Industry Applications, vol. 54, no. 6, pp. 5988-5997, Nov. 2018.

[12] Y. Gritli, A. O. Di Tommaso, R. Miceli, F. Filippetti, and C. Rossi, "Vibration signature analysis for rotor broken bar diagnosis in double cage induction motor drives," 4th International Conference on Power Engineering, Energy and Electrical Drives, Istanbul, 2013, pp. 1814-1820.

[13] C. Concari, G. Franceschini, and C. Tassoni, "Differential Diagnosis Based on Multivariable Monitoring to Assess Induction Machine Rotor Conditions," in IEEE Transactions on Industrial Electronics, vol. 55, no. 12, pp. 4156-4166, Dec. 2008.

[14] Katalin Ágoston, 'Fault Detection of the Electrical Motors based on Vibration Analysis', Procedia Technology, vol 19, p 547-553, 2015.

[15] J. Martinez, and A. Belahcen "Analysis of the Vibration Magnitude of an Induction Motor with Different Numbers of Broken Bars," in IEEE Transactions on Industry Applications, vol. 53, no. 3, pp. 2711-2720, May 2017.

[16] T. Plante, A. Nejadpak, and C. Xia Yang, "Faults detection and failures prediction using vibration analysis," 2015 IEEE AUTOTESTCON, National Harbor, MD, 2015, pp. 227-231.

[17] A. Shrivastava and S. Wadhwani, "An approach for fault detection and diagnosis of rotating electrical machine using vibration signal analysis," International Conference on Recent Advances and Innovations in Engineering (ICRAIE-2014), Jaipur, 2014, pp. 1-6.

[18] Gieras, Jacek F., Chong Wang, and Joseph Cho Lai. Noise of polyphase electric motors. CRC press, 2018.

[19] M. Valavi, A. Nysveen, R. Nillsen, and T. Rølvåg, "Slot Harmonic Effect on Magnetic Forces and Vibration in Low-Speed Permanent-Magnet Machine With Concentrated Windings," in IEEE Transactions on Industry Applications, vol. 50, no. 5, pp. 3304-3313, Sept.-Oct. 2014.

[20] E. Devillers, M. Hecquet, J. Lecointe, J. L. Besnerais, and T. Lubin, "Experimental Benchmark for Magnetic Noise and Vibrations Analysis in Electrical Machines," 2018 XIII International Conference on Electrical Machines (ICEM), Alexandroupoli, 2018, pp. 745-751.

[21] M. Babaei, J. Faiz, B. M. Ebrahimi, S. Amini, and J. Nazarzadeh, "A Detailed Analytical Model of a Salient-Pole Synchronous Generator Under Dynamic Eccentricity Fault," in IEEE Transactions on Magnetics, vol. 47, no. 4, pp. 764-771, April 2011.

[22] X. Tu, L. Dessaint, M. El Kahel, and A. O. Barry, "A New Model of Synchronous Machine Internal Faults Based on Winding Distribution," in IEEE Transactions on Industrial Electronics, vol. 53, no. 6, pp. 1818-1828, Dec. 2006.

[23] ANSYS Maxwell, Released 2019 R.3.7. ANSYS Inc.

[24] ANSYS Mechanical, Released 2019 R.3.7. ANSYS Inc.